JACS
JOURNAL OF THE AMERICAN CHEMICAL SOCIETY
pubs.acs.org/JACS
Article

Humidity-Mediated Dual Ionic–Electronic Conductivity Enables High Sensitivity in MOF Chemiresistors

Young-Moo Jo, Dong-Ha Kim, Jiande Wang, Julius J. Oppenheim, and Mircea Dincă*

Cite This: J. Am. Chem. Soc. 2024, 146, 20213–20220
Read Online
ACCESS | Metrics & More | Article Recommendations | Supporting Information

ABSTRACT: In the presence of water, the electrically conductive metal–organic framework (MOF) Cu_3HHTT_2 (H_6HHTT = 2,3,7,8,12,13-hexahydroxy-4b1,5,10,15-tetraazanaphtho[1,2,3-gh]-tetraphene) provides a conduit for proton transport, thereby becoming a dual ionic–electronic conductor. Owing to its dual conducting nature and its high density of imine and open metal sites, the MOF operates as a particularly sensitive chemiresistor, whose sensing mechanism changes with relative humidity. Thus, the interaction of NH_3 gas with the MOF under low humidity promotes proton transport, which translates to high sensitivity for ammonia detection. Conversely, NO_2 gas hinders proton conductivity, even under high relative humidity conditions, leading to large resistance variations in the humid regime. This dual ionic–electronic conduction-based gas sensor provides superior sensitivity compared to other conventional chemiresistors under similar conditions and highlights its potential as a platform for room-temperature gas sensors.

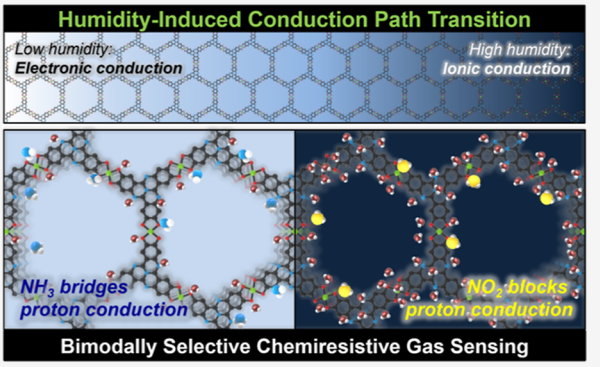

INTRODUCTION

Chemiresistive gas sensors are necessary for the detection of various airborne chemicals in the environment, factories, laboratories, agricultural locations, and households.[1,2] Although metal oxide gas sensors that operate at high temperatures have been widely used for their outstanding performance, recent advances in the Internet of Things and wireless communication technology have led to an increased demand for low-power gas sensors that operate with minimal energy consumption. To address these demands, room-temperature gas sensors have been explored utilizing carbon nanotubes,[3,4] graphene,[5−7] transition metal dichalcogenides,[6−9] phosphorene,[10] and MXenes.[11,12] However, achieving highly sensitive, selective, and reversible sensing performance at ambient temperature for chemiresistors remains challenging. Developing new chemiresistive materials with numerous gas reaction sites for higher sensitivity and with functional groups or even different mechanisms that discriminate between analytes to increase selectivity is an important goal for the field.

Electrically conducting metal–organic frameworks (cMOFs) have been gaining attention as room-temperature gas sensing materials due to facile preparation, high surface area, tunable catalytic properties, and high conductivity.[13,14] Despite the great variety of cMOFs that have been developed toward sensing applications,[15−22] the sensitivity and response–recovery rates for these materials, especially under humid environments, remain underdeveloped. In general, water molecules displace the gas reaction sites of the chemiresistors, resulting in a significant reduction in the sensitivity. Intriguingly, some cMOFs utilize the Brønsted acidic properties of adsorbed H_2O to use them as gas reaction sites,[22] suggesting that water can contribute to enhancing performance, as shown for instance with CO_2 sensors made from $Cu_3(HIB)_2$ (H_6HAB = hexaaminobenzene).[17] Inspired by these studies and by recent demonstrations of the utility of water in further enhancing surface reactivity of other materials including graphene and metal oxides through ionic conduction,[23−25] we sought to explore the possibility of enabling dual ionic–electronic conductivity in cMOFs. Indeed, we show that relative humidity (RH) can enable proton percolation and transport under certain conditions and that the dual ionic–electronic cMOFs serve as a unique platform for chemical sensing with a reporting mechanism that switches with RH.

Herein, we present a new type of cMOF chemiresistors made from Cu_3HHTT_2 (H_6HHTT = 2,3,7,8,12,13-hexahydroxy-4b1,5,10,15-tetraazanaphtho[1,2,3-gh]tetraphene). This framework crystallizes into a two-dimensional hexagonal net, where the pyridinic nitrogen and copper biscatechol reaction sites are exposed to the pore.[26] Furthermore, the abundant gas

Received: April 18, 2024
Revised: June 20, 2024
Accepted: June 25, 2024
Published: July 10, 2024

https://doi.org/10.1021/jacs.4c05343
J. Am. Chem. Soc. 2024, 146, 20213–20220

reaction sites promote water adsorption with strong hydrogen bonding, causing a transition of the conduction mechanism from electronic to proton upon water sorption. This humidity-mediated proton conduction causes the unique sensing performance to depend on the RH level. NH_3 gas, which acts as a hydrogen bond donor and acceptor, enhances responses by significantly increasing proton conductivity at RH < 25%. Conversely, NO_2 interrupts proton conduction and leads to a dramatic increase in resistance at high RH.

RESULTS AND DISCUSSION

Synthesis and Humidity-Dependent Characterization of Cu_3HHTT_2. The honeycomb layer-structured Cu_3HHTT_2 was synthesized according to a reported procedure (see the Supporting Information).[26] Cu^{2+} ions bind to oxygen atoms pertaining to catechol units to form planar, stacked 2D sheets (Figure 1a). Powder X-ray diffraction (PXRD) patterns

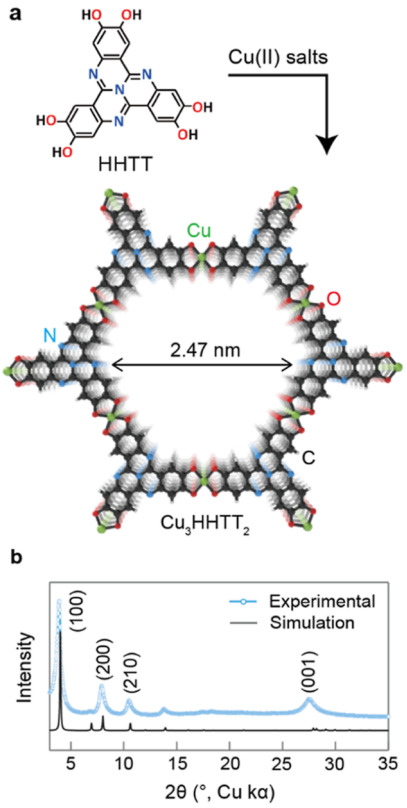

Figure 1. (a) Part of the structure of Cu_3HHTT_2 and (b) PXRD pattern of Cu_3HHTT_2.

confirmed the formation of crystalline structures with strong peaks at 3.91 and 7.93° attributed to the (100) and (200) planes, respectively (Figure 1b). The existence of Cu, C, O, and N atoms was confirmed by X-ray photoelectron spectroscopy (XPS) (Figure S1). As is often the case with other cMOFs, Cu exists as mixed valence states of Cu^+ and Cu^{2+}, confirmed by high-resolution XPS in the vicinity of the Cu 2p peaks. In the O 1s spectrum, a peak corresponding to adsorbed H_2O is prominently observed in comparison with that from lattice oxygen. In addition, both pyridinic and graphitic N of HHTT ligands are found by deconvolution of N 1s peaks. Scanning electron microscopy (SEM) images revealed hexagonal nanorods, consistent with the morphology of other 2D cMOFs (Figure S2). Fitting an N_2 adsorption isotherm measured at 77 K to the Brunauer–Emmett–Teller model gave a specific surface area of 672 ± 12 $m^2\ g^{-1}$ (Figure S3). As control groups for comparing the gas-sensing response of Cu_3HHTT_2, various triphenylene-based cMOFs were also synthesized and characterized according to the reported procedures: M_3HHTP_2 (M= Cu, Ni, Co; HHTP = 2,3,6,7,10,11-hexahydroxytriphenylene) and M_3HITP_2 (M= Cu, Ni, Co; HITP = 2,3,6,7,10,11-hexaiminotriphenylene) (Figures S4 and S5).

Slurries of Cu_3HHTT_2 were prepared at a concentration of 2 mg mL^{-1} and drop-cast onto Au-interdigitated electrodes to make individual chemiresistive sensing devices. The thicknesses of the cMOF films were adjusted by the number of droplets (n = 1, 2, 4, 8, 12, and 16) or the volume of a single droplet (n = 0.2 and 0.5) (Table S1 and Figure S6). For example, the maximum thickness of convex Cu_3HHTT_2 coatings for n = 4 and n = 16 was approximately ∼113 and ∼385 μm, respectively. In addition, a control group of other cMOF sensors was prepared with optimized film conditions for each sensing material (Table S2). The gas sensing tests were conducted using a homemade gas flow system (Figure S7). The resistance in air (R_a) of Cu_3HHTT_2-n (n = 0.2, 0.5, 1, 2, 4, 8, 12, and 16), MHHTP, and MHITP (M=Cu, Ni, Co) sensors was measured under different RH levels from dry to 70% RH using at least 3 sensors for reliable results (Figure 2).

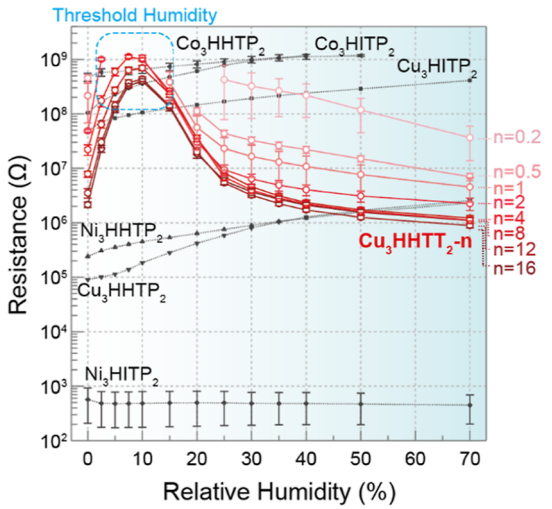

Figure 2. Humidity-dependent resistance variation of Cu_3HHTT_2 and other triphenylene-based MOF sensors.

Intriguingly, even though the overall resistance measured for each Cu_3HHTT_2-n sensor consistently increased with decreasing cMOF thickness at any RH value, each individual sensor exhibited prominent variations in resistance as a function of RH regardless of cMOF thickness: R_a fluctuated significantly. This behavior is unusual and is initially likely due to water molecules decreasing the charge carrier density with the MOF, thereby increasing the resistance.[27] We attribute the subsequent decrease in resistance above 10% RH to the formation of a continuous hydrogen bonding lattice made from adsorbed water molecules, which provides an efficient proton conduction pathway that compensates for the diminishing electronic conduction at high RH. This behavior is unique to Cu_3HHTT_2: the other cMOF devices show only slight changes in resistance across all RH ranges.

https://doi.org/10.1021/jacs.4c05343
J. Am. Chem. Soc. 2024, 146, 20213–20220

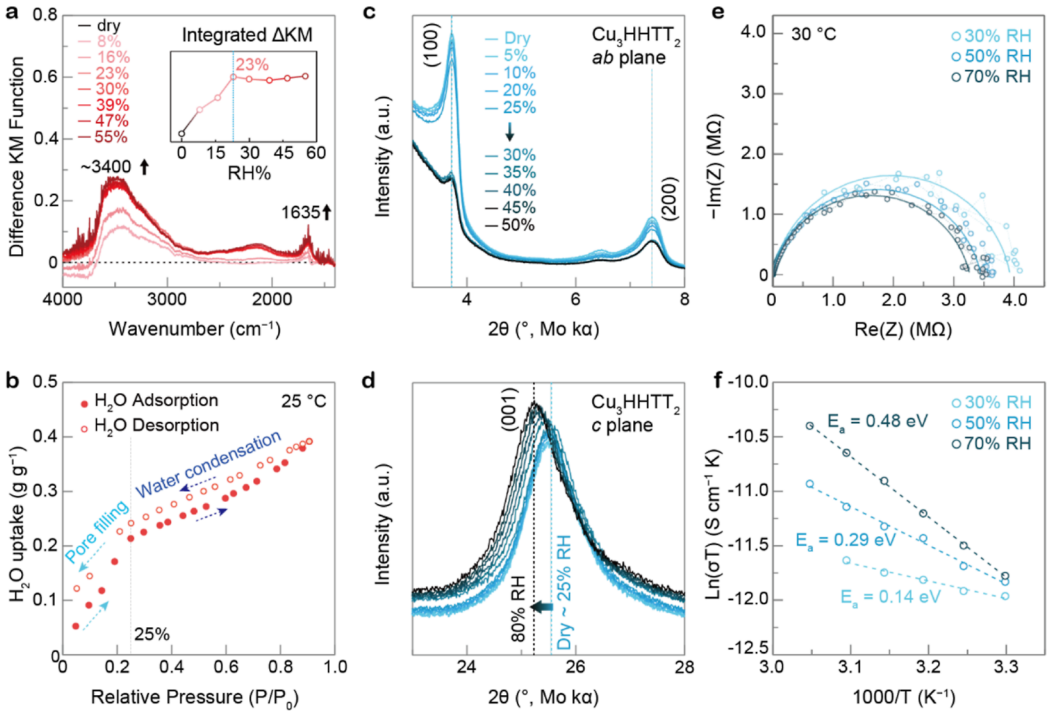

Figure 3. (a) Difference Kubelka–Munk-transformed DRIFTS spectra of Cu_3HHTT_2 as a function of RH. (b) H_2O adsorption isotherms of Cu_3HHTT_2 at 25 °C. (c,d) Humidity-dependent XRD patterns of Cu_3HHTT_2. (e) Electrochemical impedance spectra of Cu_3HHTT_2 under 30, 50, and 70% RH at 30 °C. (f) Temperature-dependent conductivity plots.

Diffuse reflectance infrared spectroscopy (DRIFTS) analysis provided a partial understanding of the mechanism governing the interaction of water molecules with Cu_3HHTT_2 (Figure 3a). As the RH increases, two intense water-related bands appear: a broad, asymmetric O–H stretching band centered around 3400 cm^{-1} and an HOH scissoring mode at 1635 cm^{-1}.[28] The intensity of both of these bands is maximized at approximately 23% RH, suggesting that water saturates the strongly adsorbing sites of Cu_3HHTT_2 below this humidity level (Figure 3a, inset). Indeed, a water adsorption isotherm conducted on Cu_3HHTT_2 activated at 120 °C exhibits a steep slope below 25% RH, with a much shallower uptake corresponding to pore condensation above this humidity level (Figure 3b).

Humidity-dependent PXRD analysis provided additional insights into the behavior and integrity of Cu_3HHTT_2 under humid conditions (Figure S8). Relevant changes pertain to shifts in the (100) and (200) peaks, corresponding to structural changes in the (*ab*) crystallographic plane (Figure 3c), and the (001) peak, reflecting changes in the stacking direction, *c*, normal to the 2*D* planes (Figure 3d). The intensity of the (100) and (200) peaks notably decreases upon hydration, especially above 25%, and is regained upon dehydration, but their positions remain constant at 3.72 and 7.40°, respectively (Figure 3c). In contrast, the (001) peak does not lose intensity but instead gradually shifts from 25.52° at low humidity (1–25% RH) toward lower 2θ angles as the humidity increases from 30 to 80% RH (Figure 3d). Altogether, the PXRD data suggest that water associating with the pyridinic nitrogen atoms and/or the Cu atoms in Cu_3HHTT_2 introduces distortions or corrugations that reversibly disrupt the long-range translational symmetry in the (*ab*) plane without changing the *a* or *b* unit cell parameters while also swelling the MOF in the *c* direction so as to increase the *d* spacing between layers.

Electrochemical impedance spectroscopy (EIS) provided initial evidence that proton conduction plays a pivotal role in the humidity-dependent resistance fluctuation of the Cu_3HHTT_2 devices. EIS spectra of Cu_3HHTT_2 above 30% RH exhibit characteristic semicircles that give conductivity values of 2.10×10^{-8} S cm^{-1} at 30% RH, 2.40×10^{-8} S cm^{-1} at 50% RH, and 2.54×10^{-8} S cm^{-1} at 70% RH (Figure 3e), proving the ionic conduction changes with RH. Measuring EIS spectra at temperatures ranging from 25 to 55 °C under varying RH conditions further provided values for the activation energy (E_a) for proton transport (Figure 3f). At 30% RH, in the early stage of water condensation, the E_a is 0.14 eV, a relatively low value suggestive of a Grotthuss mechanism.[29] With increasing humidity, the E_a for proton transport in Cu_3HHTT_2 rises to 0.29 eV at 50% RH and further to 0.48 eV at 70% RH. This trend is contrary to other MOFs, where increasing water content within a material generally decreases the E_a as the establishment of a continuous hydrogen bond network switches transport from a vehicular mechanism with $E_a > 0.4$ eV to a Grotthuss hopping mechanism with $E_a < 0.4$ eV.[28] The inverse phenomenon observed with Cu_3HHTT_2 is sometimes seen with hydrophilic 2D materials that suffer structural distortions upon water sorption.[30] Here, the distortions associated with the increase in the interlayer *d*-spacing and decrease in in-plane crystallinity are likely responsible for a disruption of the hydrogen-bonded network initially available at approximately 25–30% RH (Figure 3c,d) and the subsequent increase in E_a at higher RH (Figure 3f).

Gas-Sensing Characteristics. Given the data discussed above, the humidity response of Cu_3HHTT_2 can be divided into three distinct regions (Figure 4): the dry region where the

https://doi.org/10.1021/jacs.4c05343
J. Am. Chem. Soc. 2024, 146, 20213–20220

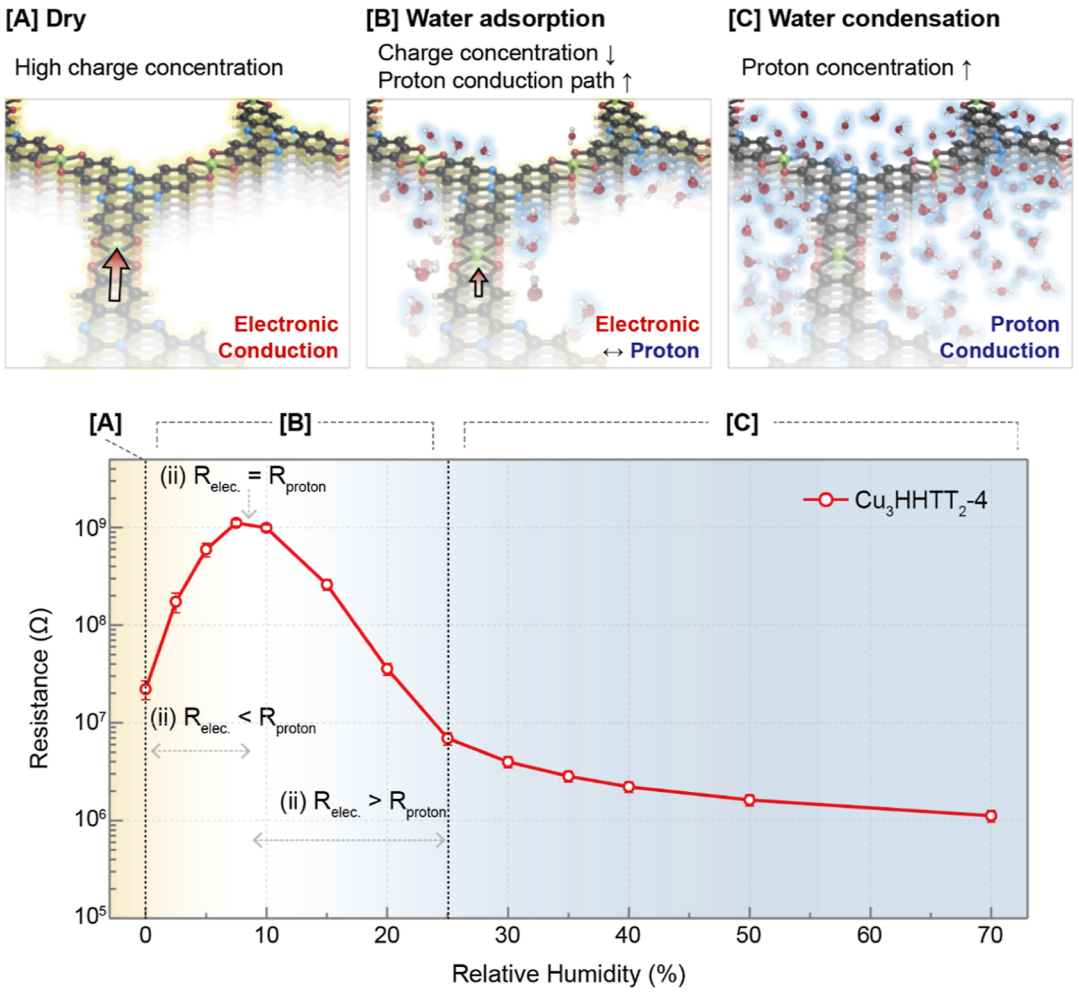

Figure 4. Conduction mechanism of Cu_3HHTT_2 sensors depending on the three different humidity regions: (a) dry condition, (b) water adsorption region, and (c) water condensation region.

analyte binding sites are fully exposed to the environment (region A); the threshold humidity region (RH < 25%, region B) where the analyte binding sites are partially occupied but not saturated with water molecules; and the water condensation region (RH > 25%, region C), where strong analyte binding sites are saturated with water, and where water molecules continue to accumulate within the MOF. Taken together, these unique humidity-dependent changes in the electrical and chemical properties of Cu_3HHTT_2 suggest the potential for new chemiresistive gas-sensing mechanisms.

To test the gas-sensing properties of Cu_3HHTT_2, we exposed Cu_3HHTT_2-*n* (*n* = 1, 2, 4, 8, 12, and 16) sensors to NH_3 (60 ppm), NO_2 (3 ppm), and various interference gases including H_2S (3 ppm), ethanol (158 ppm), acetone (823 ppm), methanol (390 ppm), benzene (269 ppm), and toluene (143 ppm) under varying humidity conditions (0−70% RH) at room temperature (~25 °C). The response (*S*) was calculated as $(R_g - R_a)/R_a$ or $(R_g - R_a)/R_g$, where R_g is resistance in gas, depending on positive or negative resistance variation, respectively.

NH_3 Sensing. The sensing transients of Cu_3HHTT_2-*n* sensors exposed to 60 ppm of NH_3 were dynamically changed depending on the RH level (Figure S9). To clarify the NH_3 sensing behavior, R_a and R_g values of Cu_3HHTT_2-*n* sensors were selected from transients in Figure S9 and plotted vs RH (Figure S10). An illustrative case is shown for the Cu_3HHTT_2-4 sensors in Figure 5. These exhibit a positive response variation to NH_3 under dry conditions (Figure 5b). Such a response with NH_3 is generally associated with *p*-type materials, as NH_3 is said to be extracting holes from the sensing material, thereby decreasing the number of charge carriers,[31] formally:

$$NH_{3(gas)} + h^+ = NH_3^+{}_{(ads)} \quad (1)$$

When the humidity increases to 10% RH, the response of *S* to ammonia becomes negative and gains magnitude (*S* = −74.4) (Figure 5b,c). The shift in absolute response to ammonia, indicative of a decrease in resistance, comes despite the depletion of charge carriers by ammonia (vide supra). It must therefore indicate a significant contribution from proton conduction even at this intermediate RH where water does not yet saturate the MOF and thus cannot provide a full proton conduction pathway on its own. Instead, ammonia, as a good hydrogen-bond donor and acceptor, likely itself contributes to the formation of interconnections between short-range hydrogen-bonded adsorbed water molecules, thereby enhancing proton conduction and an overall decrease in resistance (Figure 4, region B). Therefore, although exposure of Cu_3HHTT_2 to NH_3 does decrease the intrinsic charge carrier density of the MOF and reduces its electronic conductivity, it simultaneously drastically increased the proton

https://doi.org/10.1021/jacs.4c05343
J. Am. Chem. Soc. 2024, 146, 20213−20220

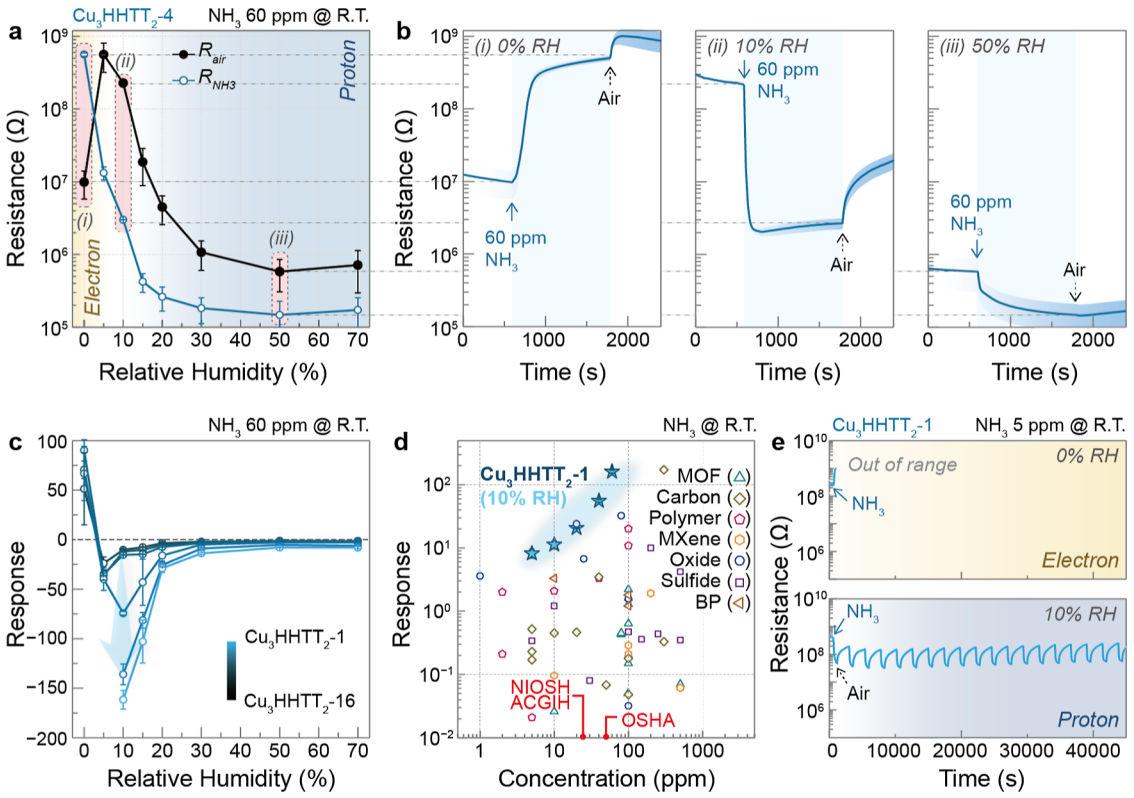

Figure 5. (a) Resistance in air (R_a) and in NH_3 (R_{NH3}) of Cu_3HHTT_2-4 sensors under different RH %. (b) Dynamic gas-sensing transients of Cu_3HHTT_2-4 sensors to 60 ppm of NH_3 at room temperature under (i) dry, (ii) 10% RH, and (iii) 50% RH. (c) Gas responses of Cu_3HHTT_2-*n* (*n* = 1, 2, 4, 8, 12, and 16) sensors to 60 ppm of NH_3 under different RH %. (d) Benchmark of reported NH_3 sensors. (e) Cyclic tests of Cu_3HHTT_2-1 sensors to 5 ppm of NH_3 under dry and 10% RH for 19 cycles.

conductivity, which compensates for the loss in electronic transport. In addition, the recovery rate of Cu_3HHTT_2-4 sensors to NH_3 is much more rapid at 10% RH than in dry conditions (Figure 5b). This can be attributed to the fact that the hydrogen bonding of NH_3 with water in humid conditions is weaker and more reversible than the direct binding of NH_3 with Cu_3HHTT_2 in dry conditions.[32] Finally, as the ambient humidity further increases above >25% RH, the response of Cu_3HHTT_2-4 sensors to NH_3 decreases precipitously (Figure 5b), presumably because the saturated water network is now self-sufficient with respect to proton transport and responds only minimally to extraneous NH_3.

The response of Cu_3HHTT_2-4 sensors is qualitatively similar in all Cu_3HHTT_2-*n* sensors, but the magnitude of the response to NH_3 was much greater for devices with thinner MOF coatings (Figure 5c). For instance, the response of Cu_3HHTT_2-1 sensors to 60 ppm of NH_3 was exceptionally high ($S = -161.6$) at 10% RH, approximately 15.7 times higher than those of Cu_3HHTT_2-16 sensors ($S = -10.3$). In addition, Cu_3HHTT_2-1 sensors exhibit high NH_3 selectivity over potential interfering gases including H_2S, ethanol, methanol, acetone, benzene, and toluene at 10% RH (Figure S11). For example, the response of Cu_3HHTT_2-1 sensors to NH_3 was 20-fold higher than its response to H_2S ($S = -8.0$) and 64 times higher than its response to 823 ppm of acetone ($S = 2.5$). This differential response and sensitivity outperform recently reported room-temperature NH_3 gas sensors comprising various chemiresistive material including MOFs, carbon-based materials, polymers, MXenes, oxides, sulfides, and black phosphorus (Figures 5d, S12, and Table S3). Moreover, the Cu_3HHTT_2-1 sensors exhibit high responses even at low NH_3 concentrations, enabling reliable and rapid detection below the permissible exposure limits of 25 and 50 ppm for up to 8 h, as stipulated by the American Conference of Governmental Industrial Hygienists (ACGIH), National Institute for Occupational Safety and Health (NIOSH), and the Occupational Safety and Health Administration (OSHA) (Figure 5d).

Importantly, Cu_3HHTT_2-*n* (*n* = 1, 2, 4, 8, and 16) sensors exhibit an irreversible behavior in dry environments, but they are stable and reversible at 10% RH (Figures 5e and S13), which is a more realistic scenario. Although the response of pristine Cu_3HHTT_2 sensors decreases at higher RH, we note that the threshold humidity can be shifted from 10 to 70% RH by adjusting the operating temperature of the sensor to 80 °C (Figure S14). We assume that the elevated temperature increases electronic conductivity and decreases proton conductivity by accelerating water desorption, thus shifting the threshold humidity level. Other common modifications, such as overlayer coatings[33,34] or grafting of hydrophobic chains,[35] may further tune the operational humidity threshold of Cu_3HHTT_2 sensors.

NO_2 Sensing. Cu_3HHTT_2-*n* sensors were also exposed to 3 ppm of NO_2 under varying humidity conditions (Figures S15 and S16). Under dry conditions, where the intrinsic electronic conduction path is dominant, Cu_3HHTT_2-4 sensors exhibit negative responses, expected for *p*-type materials in the presence of strong oxidizing analytes such as NO_2, which increase the charge carrier density (Figure 6b), which exhibit irreversible reaction due to high desorption energy of NO_2 with MOF.[36] At threshold humidity (i.e., RH < 25%), the responses of Cu_3HHTT_2-4 sensors to NO_2 were negligibly

https://doi.org/10.1021/jacs.4c05343
J. Am. Chem. Soc. 2024, 146, 20213−20220

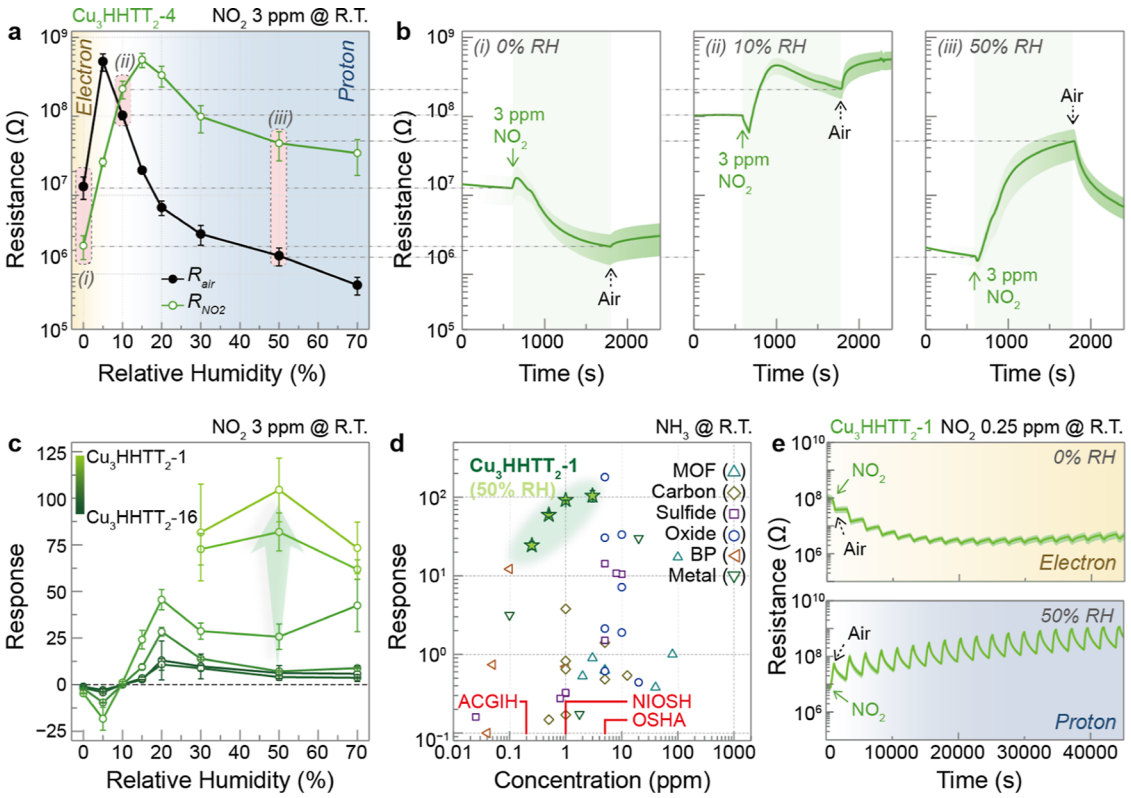

Figure 6. (a) Resistance in air (R_a) and in NO_2 (R_{NO2}) of Cu_3HHTT_2-4 sensors under different RH. (b) Dynamic gas-sensing transients of Cu_3HHTT_2-4 sensors to 3 ppm of NO_2 at room temperature under (i) dry, (ii) 10% RH, and (iii) 50% RH. (c) Gas responses of Cu_3HHTT_2-*n* (*n* = 1, 2, 4, 8, 12, and 16) sensors to 3 ppm of NO_2 under different RH %. (d) Benchmark of reported NH_3 sensors. (e) Cyclic tests of Cu_3HHTT_2-1 sensors to 0.25 ppm of NO_2 under dry and 10% RH for 19 cycles.

low. This apparent lack of response may be attributed to two competing NO_2 interactions. On one hand, NO_2 increases electronic conductivity, as explained above. On the other hand, it reduces proton conductivity in this intermediate humidity because it does not complete a hydrogen bonding network in the way that NH_3 does; in fact, it likely reacts with water, further disrupting the incipient hydrogen-bonded network. These competitive phenomena offset each other with respect to a chemiresistive response and can appear in sensing transients as fluctuations during NO_2 sensing and recovery (Figure 6b). Interestingly, the sensitivity of Cu_3HHTT_2-4 sensors toward NO_2 increases dramatically above 25% RH. We assign this response to a disruption of the robust hydrogen-bonded network and water saturation conditions: even trace amounts of NO_2 react with H_2O,[37] drastically increasing overall resistance. Importantly, the response to NO_2 is reversible: in the absence of NO_2, high humidity immediately replenishes the water network and re-establishes proton conduction and lowering the resistance of the Cu_3HHTT_2 devices (Figure 6e).

Ex situ XPS analysis of Cu_3HHTT_2 sensors before and after injection with NO_2 provided important insights into the mechanisms for the NO_2 sensing. First, the Cu 2p peaks clearly showed that NO_2 is adsorbed and oxidizes the Cu sites, as indicated by a decrease of the Cu^+/Cu^{2+} integrated peak ratio from 0.72 to 0.20 after NO_2 injection (Figure S17). Additionally, the N 1s region of the spectrum exhibits peaks corresponding to NO_3^- and NO_2^- at 405.0 and 402.4 eV, respectively (Figure S18), as would be expected through the reaction of NO_2 with water

$$NO_{2(gas)} + H_2O = HNO_{3(ads)} + HNO_{2(ads)} \quad (2)$$

As was the case with NH_3, the magnitude of the response to NO_2 was much greater for devices with thinner MOF coatings, with the response of Cu_3HHTT_2-1 sensors to 3 ppm of NO_2 being the highest (S = 104.5) (Figure 6c). Notably, Cu_3HHTT_2-1 sensors exhibit extremely high selectivity over potential interference gases including H_2S, ethanol, methanol, acetone, benzene, and toluene at 50% RH (Figure S19). These stand out among leading room-temperature chemiresistors and meet the minimum exposure threshold of various institutions including ACGIH, NIOSH, and OSHA (Figures 6d, S20, and Table S4). Again, even though Cu_3HHTT_2-*n* (*n* = 1, 2, 4, 8, and 16) sensors exhibited irreversible NO_2 binding under dry conditions, their reversibility and response magnitude increase dramatically at 50% RH (Figures 6e and S21), a more realistic scenario. This highlights the feasibility of Cu_3HHTT_2 sensors in real-world environments, where humidity is present.

CONCLUSIONS

The results here highlight the controlled fashion in which humidity generates ion−proton conduction pathways in conjunction with the electronic conduction pathways that are inherent to 2D cMOFs. This dual mechanism of charge transport enables the elaboration of sensitive and selective room-temperature chemiresistors from Cu_3(hexahydroxytetraazanaphthotetraphene)$_2$. The devices stand out in that they have a humidity-mediated response that discriminates between different gaseous molecules with extreme sensitivity. NH_3, serving as a mediator for proton transport, enables proton conduction at low humidity (10% RH). Conversely, NO_2

https://doi.org/10.1021/jacs.4c05343
J. Am. Chem. Soc. 2024, 146, 20213−20220

blocks established water-based hydrogen-bonding networks, impeding proton conduction at higher humidity (30−70% RH). The differentiated sensing mechanism for NH_3 and NO_2 is responsible for state-of-the-art sensitivity relative to other chemiresistors and high selectivity over various interference gases (H_2S, ethanol, methanol, acetone, benzene, and toluene). Notably, the sensors are reversible and have a reliable response even in high humidity environments. Fundamentally, we conclude that these results offer a blueprint for other sensor applications that make use of cMOFs and their uniquely tunable nature.

■ ASSOCIATED CONTENT

Supporting Information

The Supporting Information is available free of charge at https://pubs.acs.org/doi/10.1021/jacs.4c05343.

Additional experimental details, materials, methods, and characterization data, XPS, SEM, N_2 isotherms, PXRD, and photographs (PDF)

■ AUTHOR INFORMATION

Corresponding Author

Mircea Dincă − *Department of Chemistry, Massachusetts Institute of Technology, Cambridge, Massachusetts 02139, United States;* orcid.org/0000-0002-1262-1264; Email: mdinca@mit.edu

Authors

Young-Moo Jo − *Department of Chemistry, Massachusetts Institute of Technology, Cambridge, Massachusetts 02139, United States;* orcid.org/0000-0001-6348-7547

Dong-Ha Kim − *Department of Chemistry, Massachusetts Institute of Technology, Cambridge, Massachusetts 02139, United States;* Present Address: Department of Materials Science and Chemical Engineering, Hanyang University, Ansan 15588, Republic of Korea

Jiande Wang − *Department of Chemistry, Massachusetts Institute of Technology, Cambridge, Massachusetts 02139, United States*

Julius J. Oppenheim − *Department of Chemistry, Massachusetts Institute of Technology, Cambridge, Massachusetts 02139, United States;* orcid.org/0000-0002-5988-0677

Complete contact information is available at: https://pubs.acs.org/10.1021/jacs.4c05343

Notes

The authors declare no competing financial interest.

■ ACKNOWLEDGMENTS

This research was supported by the Department of Energy, Office of Science, Basic Energy Sciences through an award to M.D. (DOE DE-SC0023288). We thank Dr. Justin L. Andrews for assistance with EIS measurements.

■ REFERENCES

(1) Jeong, S.-Y.; Kim, J.-S.; Lee, J.-H. Rational Design of Semiconductor-Based Chemiresistors and their Libraries for Next-Generation Artificial Olfaction. *Adv. Mater.* **2020**, *32*, 2002075.

(2) Yamazoe, N. New approaches for improving semiconductor gas sensors. *Sens. Actuators B Chem.* **1991**, *5*, 7−19.

(3) Schroeder, V.; Savagatrup, S.; He, M.; Lin, S.; Swager, T. M. Carbon Nanotube Chemical Sensors. *Chem. Rev.* **2019**, *119*, 599−663.

(4) Kauffman, D. R.; Star, A. Carbon Nanotube Gas and Vapor Sensors. *Angew. Chem., Int. Ed.* **2008**, *47*, 6550−6570.

(5) Llobet, E. Gas sensors using carbon nanomaterials: A review. *Sens. Actuators B Chem.* **2013**, *179*, 32−45.

(6) Liu, X.; Ma, T.; Pinna, N.; Zhang, J. Two-Dimensional Nanostructured Materials for Gas Sensing. *Adv. Funct. Mater.* **2017**, *27*, 1702168.

(7) Anichini, C.; Czepa, W.; Pakulski, D.; Aliprandi, A.; Ciesielski, A.; Samori, P. Chemical sensing with 2D materials. *Chem. Soc. Rev.* **2018**, *47*, 4860−4908.

(8) Ping, J.; Fan, Z.; Sindoro, M.; Ying, Y.; Zhang, H. Recent Advances in Sensing Applications of Two-Dimensional Transition Metal Dichalcogenide Nanosheets and Their Composites. *Adv. Funct. Mater.* **2017**, *27*, 1605817.

(9) Kim, Y.; Lee, S.; Song, J.-G.; Ko, K. Y.; Woo, W. J.; Lee, S. W.; Park, M.; Lee, H.; Lee, Z.; Choi, H.; Kim, W.-H.; Park, J.; Kim, H. 2D Transition Metal Dichalcogenide Heterostructures for p- and n-Type Photovoltaic Self-Powered Gas Sensor. *Adv. Fucnt. Mater.* **2020**, *30*, 2003360.

(10) Abbas, A. N.; Liu, B.; Chen, L.; Ma, Y.; Cong, S.; Aroonyadet, N.; Köpf, M.; Nilges, T.; Zhou, C. Black Phosphorus Gas Sensors. *ACS Nano* **2015**, *9*, 5618−5624.

(11) Kim, S. J.; Koh, H.-J.; Ren, C. E.; Kwon, O.; Maleski, K.; Cho, S.-Y.; Anasori, B.; Kim, C.-K.; Choi, Y.-K.; Kim, J.; Gogotsi, Y.; Jung, H.-T. Metallic $Ti_3C_2T_x$ MXene Gas Sensors with Ultrahigh Signal-to-Noise Ratio. *ACS Nano* **2018**, *12*, 986−993.

(12) Meng, Z.; Stolz, R. M.; Mendecki, L.; Mirica, K. A. Electrically-Transduced Chemical Sensors Based on Two-Dimensional Nanomaterials. *Chem. Rev.* **2019**, *119*, 478−598.

(13) Xie, L. S.; Skorupskii, G.; Dincă, M. Electrically Conductive Metal-Organic Frameworks. *Chem. Rev.* **2020**, *120*, 8536−8580.

(14) Jo, Y.-M.; Jo, Y. K.; Lee, J.-H.; Jang, H. W.; Hwang, I.-S.; Yoo, D. J. MOF-Based Chemiresistive Gas Sensors: Toward New Functionalities. *Adv. Mater.* **2023**, *35*, 2206842.

(15) Campbell, M. G.; Sheberla, D.; Liu, S. F.; Swager, T. M.; Dincă, M. Cu_3(hexaiminotriphenylene)$_2$: An Electrically Conductive 2D Metal-Organic Framework for Chemiresistive Sensing. *Angew. Chem., Int. Ed.* **2015**, *54*, 4349−4352.

(16) Campbell, M. G.; Liu, S. F.; Swager, T. M.; Dincă, M. Chemiresistive Sensor Arrays from Conductive 2D Metal-Organic Frameworks. *J. Am. Chem. Soc.* **2015**, *137*, 13780−13783.

(17) Stassen, I.; Dou, J.-H.; Hendon, C.; Dincă, M. Chemiresistive Sensing of Ambient CO_2 by an Autogenously Hydrated Cu_3(hexaiminobenzene)$_2$ Framework. *ACS Cent. Sci.* **2019**, *5*, 1425−1431.

(18) Meng, Z.; Stolz, R. M.; Mirica, K. A. Two-Dimensional Chemiresistive Covalent Organic Framework with High Intrinsic Conductivity. *J. Am. Chem. Soc.* **2019**, *141*, 11929−11937.

(19) Aykanat, A.; Meng, Z.; Stolz, R. M.; Morrell, C. T.; Mirica, K. A. Bimetallic Two-Dimensional Metal-Organic Frameworks for the Chemiresistive Detection of Carbon Monoxide. *Angew. Chem., Int. Ed.* **2022**, *61*, No. e202113665.

(20) Meng, Z.; Aykanat, A.; Mirica, K. A. Welding Metallophthalocyanines into Bimetallic Molecular Meshes for Ultrasensitive, Low-Power Chemiresistive Detection of Gases. *J. Am. Chem. Soc.* **2019**, *141*, 2046−2053.

(21) Su, X.; Zhong, Z.; Yan, X.; Zhang, T.; Wang, C.; Wang, Y.-X.; Xu, G.; Chen, L. Facile Synthesis of Metallosalphen-Based 2D Conductive Metal-Organic Frameworks for NO_2 Sensing: Metal Coordination Induced Planarization. *Angew. Chem., Int. Ed.* **2023**, *62*, No. e202302645.

(22) Stolz, R. M.; Mahdavi-Shakib, A.; Frederick, B. G.; Mirica, K. A. Host-Guest Interactions and Redox Activity in Layered Conductive Metal-Organic Frameworks. *Chem. Mater.* **2020**, *32*, 7639−7652.

(23) Zhou, Y.; Wang, Y.; Wang, Y.; Li, X. Humidity-Enabled Ionic Conductive Trace Carbon Dioxide Sensing of Nitrogen-Doped

$Ti_3C_2T_x$ MXene/Polyethyleneimine Composite Films Decorated with Reduced Graphene Oxide Nanosheets. *Anal. Chem.* **2020**, *92*, 16033−16042.
(24) Song, Y. G.; Shim, Y.-S.; Suh, J. M.; Noh, M.-S.; Kim, G. S.; Choi, K. S.; Jeong, B.; Kim, S.; Jang, H. W.; Ju, B.-K.; Kang, C.-Y. Ionic-Activated Chemiresistive Gas Sensors for Room-Temperature Operation. *Small* **2019**, *15*, 1902065.
(25) Wu, Z.; Rong, L.; Yang, J.; Wei, Y.; Tao, K.; Zhou, Y.; Yang, B.-R.; Xie, X.; Wu, J. Ion-Conductive Hydrogel-Based Stretchable, Self-Healing, and Transparent NO_2 Sensor with High Sensitivity and Selectivity at Room Temperature. *Small* **2021**, *17*, 2104997.
(26) Dou, J.-H.; Arguilla, M. Q.; Luo, Y.; Li, J.; Zhang, W.; Sun, L.; Mancuso, J. L.; Yang, L.; Chen, T.; Parent, L. R.; Skorupskii, G.; Libretto, N. J.; Sun, C.; Yang, M. C.; Dip, P. V.; Brignole, E. J.; Miller, J. T.; Kong, J.; Hendon, C. H.; Sun, J.; Dincă, M. Atomically precise single-crystal structures of electrically conducting 2D metal-organic frameworks. *Nat. Mater.* **2021**, *20*, 222−228.
(27) Zahab, A.; Spina, L.; Poncharal, P.; Marlière, C. Water-vapor effect on the electrical conductivity of a single-walled carbon nanotube mat. *Phys. Rev. B* **2000**, *62*, 10000−10003.
(28) Mojet, B. L.; Ebbesen, S. D.; Lefferts, L. Light at the interface: the potential of attenuated total reflection infrared spectroscopy for understanding heterogeneous catalysis in water. *Chem. Soc. Rev.* **2010**, *39*, 4643−4655.
(29) Lim, D.-W.; Kitagawa, H. Proton Transport in Metal-Organic Frameworks. *Chem. Rev.* **2020**, *120*, 8416−8467.
(30) Zhang, L.; Liu, Z.; Yang, C.; García Sakai, V.; Tyagi, M.; Hong, L. Conduction Mechanism in Graphene Oxide Membranes with Varied Water Content: From Proton Hopping Dominant to Ion Diffusion Dominant. *ACS Nano* **2022**, *16* (9), 13771−13782.
(31) Wang, X.; Li, X.; Zhang, L.; Yoon, Y.; Weber, P. K.; Wang, H.; Guo, J.; Dai, H. N-Doping of Graphene Through Electrothermal Reactions with Ammonia. *Science* **2009**, *324* (5928), 768−771.
(32) Kollman, P.; Mckelvey, J.; Johansson, A.; Rothenberg, S. Theoretical studies of hydrogen-bonded dimers. Complexes involving HF, H_2O, NH_3, HCl, H_2S, PH_3, HCN, HNC, HCP, CH_2NH, H_2CS, H_2CO, CH_4, CF_3H, C_2H_2, C_2H_4, C_6H_6, F^-, and H_3O^+. *J. Am. Chem. Soc.* **1975**, *97* (5), 955−965.
(33) Jang, J.-S.; Jung, H. J.; Chong, S.; Kim, D.-H.; Kim, J.; Kim, S. O.; Kim, I.-D. 2D Materials Decorated with Ultrathin and Porous Graphene Oxide for High Stability and Selective Surface Activity. *Adv. Mater.* **2020**, *32*, 2002723.
(34) Li, H.-Y.; Lee, C.-S.; Kim, D. H.; Lee, J.-H. Flexible Room-Temperature NH_3 Sensor for Ultrasensitive, Selective, and Humidity-Independent Gas Detection. *ACS Appl. Mater. Interfaces* **2018**, *10*, 27858−27867.
(35) Wang, M.; Zhang, Z.; Zhong, H.; Huang, X.; Li, W.; Hambsch, M.; Zhang, P.; Wang, Z.; St Petkov, P.; Heine, T.; Mannsfeld, S. C. B.; Feng, X.; Dong, R. Surface-Modified Phthalocyanine-Based Two-Dimensional Conjugated Metal-Organic Framework Films for Polarity-Selective Chemiresistive Sensing. *Angew. Chem. Int. Ad.* **2021**, *60*, 18666−18672.
(36) Koo, W.-T.; Kim, S.-J.; Jang, J.-S.; Kim, D.-H.; Kim, I.-D. Catalytic Metal Nanoparticles Embedded in Conductive Metal-Organic Frameworks for Chemiresistors: Highly Active and Conductive Porous Materials. *Adv. Sci.* **2019**, *6* (21), 1900250.
(37) Goodman, A. L.; Underwood, G. M.; Grassian, V. H. Heterogeneous Reaction of NO_2: Characterization of Gas-Phase and Adsorbed Products from the Reaction, $2NO_2(g) + H_2O(a) \rightarrow HONO(g) + HNO_3(a)$ on Hydrated Silica Particles. *J. Phys. Chem. A* **1999**, *103*, 7217−7223.

https://doi.org/10.1021/jacs.4c05343
J. Am. Chem. Soc. 2024, 146, 20213−20220